

anticancer agents or other Hedgehog pathway inhibitors with ATO may be valuable for treating osteosarcoma patients.

Supporting Information

Figure S1. Western blot analysis showed that ATO treatment decreased the expression of phosphorylated JNK. Western blot analysis showed that ATO treatment did not affect the expression levels of NFκB and phosphorylated NFκB proteins. WST assay showed that JNK inhibitor did not affect the proliferation of osteosarcoma cells.

References

- Sweetnam R (1982) Osteosarcoma. *Br J Hosp Med* 28: 112: 116-121.
- Dorfman HD, Czerniak B (1995) Bone cancers. *Cancer* 75: 203-210. doi:10.1002/1097-0142(19950101)75:1+. PubMed: 8000997
- Iwamoto Y, Tanaka K, Isu K, Kawai A, Tatezaki S et al. (2009) Multiinstitutional phase II study of neoadjuvant chemotherapy for osteosarcoma (NECO study) in Japan: NECO-93J and NECO-95J. *J Orthop Sci* 14: 397-404. doi:10.1007/s00776-009-1347-6. PubMed: 19662473.
- Kager L, Zoubek A, Kastner U, Kempf-Bielack B, Potratz J et al. (2006) Skip metastases in osteosarcoma: experience of the Cooperative Osteosarcoma Study Group. *J Clin Oncol* 24: 1535-1541. doi:10.1200/JCO.2005.04.2978. PubMed: 16575004.
- Ingham PW, McMahon AP (2001) Hedgehog signaling in animal development: paradigms and principles. *Genes Dev* 15: 3059-3087. doi:10.1101/gad.938601. PubMed: 11731473.
- Ruiz i Altaba A, Sanchez P, Dahmane N (2002) Gli and hedgehog in cancer: tumours, embryos and stem cells. *Nat Rev Cancer* 2: 361-372.
- Lum L, Beachy PA (2004) The Hedgehog response network: sensors, switches, and routers. *Science* 304: 1755-1759. doi:10.1126/science.1098020. PubMed: 15205520.
- Ruiz i Altaba A, Mas C, Stecca B (2007) The Gli code: an information nexus regulating cell fate, stemness and cancer. *Trends Cell Biol* 17: 438-447.
- Nagao H, Ijiri K, Hirotsu M, Ishidou Y, Yamamoto T et al. (2011) Role of GLI2 in the growth of human osteosarcoma. *J Pathol* 224: 169-179. doi: 10.1002/path.2880. PubMed: 21506130.
- Hirotsu M, Setoguchi T, Sasaki H, Matsunoshita Y, Gao H et al. (2010) Smoothed as a new therapeutic target for human osteosarcoma. *Mol Cancer* 9: 5. doi:10.1186/1476-4598-9-5. PubMed: 20067614.
- Berman DM, Karhadkar SS, Hallahan AR, Pritchard JI, Eberhart CG et al. (2002) Medulloblastoma growth inhibition by hedgehog pathway blockade. *Science* 297: 1559-1561. doi:10.1126/science.1073733. PubMed: 12202832.
- Williams JA, Guicherit OM, Zaharian BI, Xu Y, Chai L et al. (2003) Identification of a small molecule inhibitor of the hedgehog signaling pathway: effects on basal cell carcinoma-like lesions. *Proc Natl Acad Sci U S A* 100: 4616-4621. doi:10.1073/pnas.0732813100. PubMed: 12679522.
- Robarge KD, Brunton SA, Castanedo GM, Cui Y, Dina MS et al. (2009) GDC-0449-a potent inhibitor of the hedgehog pathway. *Bioorg Med Chem Lett* 19: 5576-5581. doi:10.1016/j.bmcl.2009.08.049. PubMed: 19716296.
- Tremblay MR, Lescaubeau A, Grogan MJ, Tan E, Lin G et al. (2009) Discovery of a potent and orally active hedgehog pathway antagonist (IPI-926). *J Med Chem* 52: 4400-4418. doi:10.1021/jm900305z. PubMed: 19522463.
- Rudin CM, Hann CL, Laterra J, Yauch RL, Callahan CA et al. (2009) Treatment of medulloblastoma with hedgehog pathway inhibitor GDC-0449. *N Engl J Med* 361: 1173-1178. doi:10.1056/NEJMoa0902903. PubMed: 19726761.
- Xie J, Murone M, Luoh SM, Ryan A, Gu Q et al. (1998) Activating Smoothed mutations in sporadic basal-cell carcinoma. *Nature* 391: 90-92. doi:10.1038/34201. PubMed: 9422511.
- Taipale J, Chen JK, Cooper MK, Wang B, Mann RK et al. (2000) Effects of oncogenic mutations in Smoothed and Patched can be reversed by cyclopamine. *Nature* 406: 1005-1009. doi: 10.1038/35023008. PubMed: 10984056.
- Taylor MD, Liu L, Raffel C, Hui CC, Mainprize TG et al. (2002) Mutations in SUFU predispose to medulloblastoma. *Nat Genet* 31: 306-310. doi:10.1038/ng916. PubMed: 12068298.
- Tostar U, Malm CJ, Meis-Kindblom JM, Kindblom LG, Toftgård R et al. (2006) Deregulation of the hedgehog signalling pathway: a possible role for the PTCH and SUFU genes in human rhabdomyoma and rhabdomyosarcoma development. *J Pathol* 208: 17-25. doi:10.1002/path.1882. PubMed: 16294371.
- Lee Y, Kawagoe R, Sasai K, Li Y, Russell HR et al. (2007) Loss of suppressor-of-fused function promotes tumorigenesis. *Oncogene* 26: 6442-6447. doi:10.1038/sj.onc.1210467. PubMed: 17452975.
- Sheng T, Li C, Zhang X, Chi S, He N et al. (2004) Activation of the hedgehog pathway in advanced prostate cancer. *Mol Cancer* 3: 29. doi: 10.1186/1476-4598-3-29. PubMed: 15482598.
- Lengfelder E, Hofmann WK, Nowak D (2012) Impact of arsenic trioxide in the treatment of acute promyelocytic leukemia. *Leukemia* 26: 433-442. doi:10.1038/leu.2011.245. PubMed: 21904379.
- Beauchamp EM, Ringer L, Bulut G, Sajwan KP, Hall MD et al. (2011) Arsenic trioxide inhibits human cancer cell growth and tumor development in mice by blocking Hedgehog/GLI pathway. *J Clin Invest* 121: 148-160. doi:10.1172/JCI42874. PubMed: 21183792.
- Kim J, Aftab BT, Tang JY, Kim D, Lee AH et al. (2013) Itraconazole and arsenic trioxide inhibit Hedgehog pathway activation and tumor growth associated with acquired resistance to smoothened antagonists. *Cancer Cell* 23: 23-34. doi:10.1016/j.ccr.2012.11.017. PubMed: 23291299.
- Kim J, Lee JJ, Kim J, Gardner D, Beachy PA (2010) Arsenic antagonizes the Hedgehog pathway by preventing ciliary accumulation and reducing stability of the Gli2 transcriptional effector. *Proc Natl Acad Sci U S A* 107: 13432-13437. doi:10.1073/pnas.1006822107. PubMed: 20624968.
- Plesca D, Crosby ME, Gupta D, Almasan A (2007) E2F4 function in G2: maintaining G2-arrest to prevent mitotic entry with damaged DNA. *Cell Cycle* 6: 1147-1152. doi:10.4161/cc.6.10.4259. PubMed: 17507799.
- Jung HS, Kim HS, Lee MJ, Shin HY, Ahn HS et al. (2006) Arsenic trioxide concentration determines the fate of Ewing's sarcoma family tumors and neuroblastoma cells in vitro. *FEBS Lett* 580: 4969-4975. doi:10.1016/j.febslet.2006.07.077. PubMed: 16930595.
- Mathieu J, Besançon F (2006) Clinically tolerable concentrations of arsenic trioxide induce p53-independent cell death and repress NF-κB activation in Ewing sarcoma cells. *Int J Cancer* 119: 1723-1727. doi:10.1002/ijc.21970. PubMed: 16646077.
- Yang W, Liu X, Choy E, Mankin H, Hornicek FJ et al. (2012) Targeting hedgehog-GLI-2 pathway in osteosarcoma. *J Orthop Res*, 31: 502-9. PubMed: 22968906.
- Bigelow RL, Chari NS, Uden AB, Spurgers KB, Lee S et al. (2004) Transcriptional regulation of bcl-2 mediated by the sonic hedgehog signaling pathway through gli-1. *J Biol Chem* 279: 1197-1205. PubMed: 14555646.
- Regl G, Kasper M, Schnidar H, Eichberger T, Neill GW et al. (2004) Activation of the BCL2 promoter in response to Hedgehog/GLI signal transduction is predominantly mediated by GLI2. *Cancer Res* 64: 7724-7731. doi:10.1158/0008-5472.CAN-04-1085. PubMed: 15520176.
- Narita S, So A, Ettinger S, Hayashi N, Muramaki M et al. (2008) GLI2 knockdown using an antisense oligonucleotide induces apoptosis and chemosensitizes cells to paclitaxel in androgen-independent prostate cancer. *Clin Cancer Res* 14: 5769-5777. doi: 10.1158/1078-0432.CCR-07-4282. PubMed: 18794066.

(TIF)

Acknowledgements

We are grateful to Hui Gao for excellent technical assistance.

Author Contributions

Conceived and designed the experiments: TS. Performed the experiments: S. Nakamura S. Nagano HN. Analyzed the data: YI MA TY SK TS. Contributed reagents/materials/analysis tools: MY. Wrote the manuscript: SK TS.

33. Singh RR, Kunkalla K, Qu C, Schlette E, Neelapu SS et al. (2011) ABCG2 is a direct transcriptional target of hedgehog signaling and involved in stroma-induced drug tolerance in diffuse large B-cell lymphoma. *Oncogene* 30: 4874-4886. doi:10.1038/onc.2011.195. PubMed: 21625222.
34. Von Hoff DD, LoRusso PM, Rudin CM, Reddy JC, Yauch RL et al. (2009) Inhibition of the hedgehog pathway in advanced basal-cell carcinoma. *N Engl J Med* 361: 1164-1172. doi:10.1056/NEJMoa0905360. PubMed: 19726763.
35. Bisht S, Brossart P, Maitra A, Feldmann G (2010) Agents targeting the Hedgehog pathway for pancreatic cancer treatment. *Curr Opin Investig Drugs* 11: 1387-1398. PubMed: 21154121.
36. Chen JK, Taipale J, Young KE, Maiti T, Beachy PA (2002) Small molecule modulation of Smoothened activity. *Proc Natl Acad Sci U S A* 99: 14071-14076. doi:10.1073/pnas.182542899. PubMed: 12391318.
37. Roberts WM, Douglass EC, Peiper SC, Houghton PJ, Look AT (1989) Amplification of the gli gene in childhood sarcomas. *Cancer Res* 49: 5407-5413. PubMed: 2766305.
38. Khatib ZA, Matsushime H, Valentine M, Shapiro DN, Sherr CJ et al. (1993) Coamplification of the CDK4 gene with MDM2 and GLI in human sarcomas. *Cancer Res* 53: 5535-5541. PubMed: 8221695.
39. Zwerner JP, Joo J, Warner KL, Christensen L, Hu-Lieskovan S et al. (2008) The EWS/FLI1 oncogenic transcription factor deregulates GLI1. *Oncogene* 27: 3282-3291. doi:10.1038/sj.onc.1210991. PubMed: 18084326.
40. Beauchamp E, Bulut G, Abaan O, Chen K, Merchant A et al. (2009) GLI1 is a direct transcriptional target of EWS-FLI1 oncoprotein. *J Biol Chem* 284: 9074-9082. doi:10.1074/jbc.M806233200. PubMed: 19189974.
41. Nolan-Stevaux O, Lau J, Truitt ML, Chu GC, Hebrok M et al. (2009) GLI1 is regulated through Smoothened-independent mechanisms in neoplastic pancreatic ducts and mediates PDAC cell survival and transformation. *Genes Dev* 23: 24-36. doi:10.1101/gad.1753809. PubMed: 19136624.
42. Xu Y, Chenna V, Hu C, Sun HX, Khan M et al. (2011) Polymeric nanoparticle-encapsulated hedgehog pathway inhibitor HPI-1 (NanoHHI) inhibits systemic metastases in an orthotopic model of human hepatocellular carcinoma. *Clin Cancer Res* 18: 1291-1302. PubMed: 21868763.
43. Pan D, Li Y, Li Z, Wang Y, Wang P et al. (2012) Gli inhibitor GANT61 causes apoptosis in myeloid leukemia cells and acts in synergy with rapamycin. *Leuk Res* 36: 742-748. doi:10.1016/j.leukres.2012.02.012. PubMed: 22398221.
44. Mazumdar T, Devecchio J, Agyeman A, Shi T, Houghton JA (2011) Blocking Hedgehog survival signaling at the level of the GLI genes induces DNA damage and extensive cell death in human colon carcinoma cells. *Cancer Res* 71: 5904-5914. doi: 10.1158/0008-5472.CAN-10-4173. PubMed: 21747117.
45. Gafis N, Katsoulidis E, Sassano A, Tallman MS, Higgins LS et al. (2006) Role of the p38 mitogen-activated protein kinase pathway in the generation of arsenic trioxide-dependent cellular responses. *Cancer Res* 66: 6763-6771. doi:10.1158/0008-5472.CAN-05-3699. PubMed: 16818652.
46. Cavigelli M, Li WW, Lin A, Su B, Yoshioka K et al. (1996) The tumor promoter arsenite stimulates AP-1 activity by inhibiting a JNK phosphatase. *EMBO J* 15: 6269-6279. PubMed: 8947050.
47. Kapahi P, Takahashi T, Natoli G, Adams SR, Chen Y et al. (2000) Inhibition of NF-kappa B activation by arsenite through reaction with a critical cysteine in the activation loop of I kappa B kinase. *J Biol Chem* 275: 36062-36066. doi:10.1074/jbc.M007204200. PubMed: 10967126.
48. Shen ZX, Chen GQ, Ni JH, Li XS, Xiong SM et al. (1997) Use of arsenic trioxide (As2O3) in the treatment of acute promyelocytic leukemia (APL): II. Clinical efficacy and pharmacokinetics in relapsed patients. *Blood* 89: 3354-3360. PubMed: 9129042.

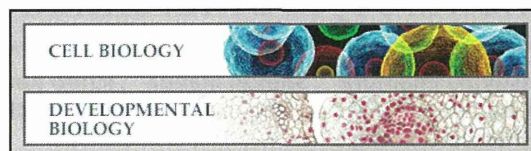
Cell Biology:

**Human Immunodeficiency Virus Type 1
Enhancer-binding Protein 3 Is Essential for
the Expression of Asparagine-linked
Glycosylation 2 in the Regulation of
Osteoblast and Chondrocyte Differentiation**

Katsuyuki Imamura, Shingo Maeda, Ichiro
Kawamura, Kanehiro Matsuyama, Naohiro
Shinohara, Yuhei Yahiro, Satoshi Nagano,
Takao Setoguchi, Masahiro Yokouchi,
Yasuhiro Ishidou and Setsuro Komiya

J. Biol. Chem. 2014, 289:9865-9879.

doi: 10.1074/jbc.M113.520585 originally published online February 21, 2014



Access the most updated version of this article at doi: [10.1074/jbc.M113.520585](https://doi.org/10.1074/jbc.M113.520585)

Find articles, minireviews, Reflections and Classics on similar topics on the JBC Affinity Sites.

Alerts:

- When this article is cited
- When a correction for this article is posted

[Click here](#) to choose from all of JBC's e-mail alerts

Supplemental material:

<http://www.jbc.org/content/suppl/2014/02/21/M113.520585.DC1.html>

This article cites 43 references, 19 of which can be accessed free at
<http://www.jbc.org/content/289/14/9865.full.html#ref-list-1>

Human Immunodeficiency Virus Type 1 Enhancer-binding Protein 3 Is Essential for the Expression of Asparagine-linked Glycosylation 2 in the Regulation of Osteoblast and Chondrocyte Differentiation^{*[5]}

Received for publication, September 20, 2013, and in revised form, January 26, 2014. Published, JBC Papers in Press, February 21, 2014, DOI 10.1074/jbc.M113.520585

Katsuyuki Imamura^{†§}, Shingo Maeda^{†1}, Ichiro Kawamura[§], Kanehiro Matsuyama^{†§}, Naohiro Shinohara^{†§}, Yuhei Yahiro^{†§}, Satoshi Nagano[§], Takao Setoguchi[¶], Masahiro Yokouchi[§], Yasuhiro Ishidou[‡], and Setsuro Komiya^{†§¶}

From the Departments of [†]Medical Joint Materials and [§]Orthopaedic Surgery and the [¶]Near-Future Locomotor Organ Medicine Creation Course, Graduate School of Medical and Dental Sciences, Kagoshima University, Kagoshima 890-8544, Japan

Background: The mechanisms by which Hivep3 regulates the osteochondrogenesis remain elusive.

Results: Knockdown of Hivep3 down-regulated *Alg2* expression. *Alg2* suppressed osteoblast differentiation by inhibiting the activity of Runx2. *Alg2* silencing suppressed the expression of *Creb3l2* and chondrogenesis.

Conclusion: *Alg2* may be a modulator of osteochondrogenesis.

Significance: This is the first report to describe the association of an *Alg* gene with osteochondrogenesis.

Human immunodeficiency virus type 1 enhancer-binding protein 3 (*Hivep3*) suppresses osteoblast differentiation by inducing proteasomal degradation of the osteogenesis master regulator Runx2. In this study, we tested the possibility of cooperation of Hivep1, Hivep2, and Hivep3 in osteoblast and/or chondrocyte differentiation. Microarray analyses with ST-2 bone stroma cells demonstrated that expression of any known osteochondrogenesis-related genes was not commonly affected by the three Hivep siRNAs. Only *Hivep3* siRNA promoted osteoblast differentiation in ST-2 cells, whereas all three siRNAs cooperatively suppressed differentiation in ATDC5 chondrocytes. We further used microarray analysis to identify genes commonly down-regulated in both MC3T3-E1 osteoblasts and ST-2 cells upon knockdown of *Hivep3* and identified asparagine-linked glycosylation 2 (*Alg2*), which encodes a mannosyltransferase residing on the endoplasmic reticulum. The *Hivep3* siRNA-mediated promotion of osteoblast differentiation was negated by forced *Alg2* expression. *Alg2* suppressed osteoblast differentiation and bone formation in cultured calvarial bone. *Alg2* was immunoprecipitated with Runx2, whereas the combined transfection of Runx2 and *Alg2* interfered with Runx2 nuclear localization, which resulted in suppression of Runx2 activity. Chondrocyte differentiation was promoted by Hivep3 overexpression, in concert with increased expression of *Creb3l2*, whose gene product is the endoplasmic reticulum stress transducer crucial for chondrogenesis. *Alg2* silencing suppressed *Creb3l2* expression and chondrogenesis of ATDC5 cells, whereas infection of *Alg2*-expressing virus promoted chondrocyte maturation in cul-

tured cartilage rudiments. Thus, *Alg2*, as a downstream mediator of Hivep3, suppresses osteogenesis, whereas it promotes chondrogenesis. To our knowledge, this study is the first to link a mannosyltransferase gene to osteochondrogenesis.

In skeletal development and bone remodeling, osteoblasts play major roles not only in bone formation but also in inducing the differentiation of bone-resorbing osteoclasts (1, 2). Runx2 is a critical transcription factor in osteoblast differentiation, as evidenced by Runx2 knock-out mice, which exhibit a complete lack of both intramembranous and endochondral ossification due to the absence of osteoblasts (3). Cleidocranial dysplasia, a human autosomal dominant inherited disorder of bone development, is characterized by hypoplasia of clavicles and abnormalities in cranial and facial bones and is caused by mutations in the *Runx2* gene (4, 5). Some genes, e.g. LDL receptor-related protein 5 (*Lrp5*), sclerostin (*Sost*), and human immunodeficiency virus type 1 enhancer-binding protein 3 (*Hivep3*), have been found to control osteoblast function in the adult human and/or mouse during postnatal skeletal remodeling (6–10).

Hivep3, also known as Schnurri-3, Zas3, and Krc, is a member of three mammalian homologs of the Hivep/Schnurri family of large zinc finger proteins. Hivep proteins have been studied for their roles in the regulation of an assortment of genes, including those encoding collagen type IIA, α A-crystallin, β -interferon, and HIV genes (11). Hivep2 can indirectly interact with the peroxisome proliferator-activated receptor γ 2 (*Pparg2*) promoter to promote adipogenesis, through binding to Smad1, an intracellular mediator of bone morphogenetic protein (BMP)² signaling. Hivep2 can also dock to CCAAT/enhancer-binding protein α (*C/ebp α*) to interact

* This work was supported by Japan Society for the Promotion of Science KAKENHI Grants 23592221 (to S. M.) and 23592222 (to Y. I.), a grant from the Cell Science Research Foundation (to S. M.), and a grant from the Hip Joint Foundation of Japan (to S. M.).

[5] This article contains supplemental Tables 1–5.

¹ To whom correspondence should be addressed: Dept. of Medical Joint Materials, Graduate School of Medical and Dental Sciences, Kagoshima University, 8-35-1 Sakuragaoka, Kagoshima 890-8544, Japan. Tel.: 81-99-275-5381; Fax: 81-99-265-4699; E-mail: maeda-s@umin.ac.jp or s-maeda@m3.kufm.kagoshima-u.ac.jp.

² The abbreviations used are: BMP, bone morphogenetic protein; ER, endoplasmic reticulum; ALP, alkaline phosphatase; ECM, extracellular matrix; CDG, congenital disorders of glycosylation; qRT, quantitative RT; ALG, asparagine-linked glycosylation.

Hivep3-dependent Alg2 Expression Inhibits Osteogenesis

with a CCAAT site on the distal part of the *Pparg* gene (12). Mice lacking Hivep3 demonstrate adult-onset osteosclerosis with increased bone volume due to enhanced osteoblast activity (10). Hivep3 promotes proteasomal degradation of the Runx2 protein through recruitment of the E3 ubiquitin ligase Wwp1 to Runx2 (10). A D-domain motif within Hivep3 mediates the interaction with and inhibition of ERK mitogen-activated protein kinase (MAPK), thereby inhibiting Wnt/Lrp5 signaling through regulation of the activity of a downstream mediator glycogen synthase kinase 3- β (Gsk3 β). This interaction results in the suppression of subsequent osteoblast differentiation (13). In addition, Hivep3 indirectly promotes osteoclastogenesis by promoting osteoblastic expression of receptor activator of nuclear factor- κ B ligand (Rankl), a crucial factor for osteoclast differentiation (14). Hivep3 also cell-autonomously promotes osteoclastogenesis by inducing the expression of *Nfatc1*, a master transcription factor in osteoclast differentiation, by interacting with Traf6 to enhance its activity while forming a complex with c-Jun to activate the *Nfatc1* promoter (15). Thus, Hivep3 controls both bone formation and resorption at multiple steps to maintain normal bone mass. However, whether Hivep3 controls gene expression in osteoblasts to regulate osteoblast activity is unclear.

In contrast to *Hivep3* knock-out mice, mice lacking *Hivep2* exhibited decreased cortical bone volume and increased cancellous bone mass (16), suggesting different roles for Hivep2 and Hivep3 in the skeleton. Combined ablation of *Hivep2* and *Hivep3* in mice resulted in synergistically increased trabecular bone volume, demonstrating a redundancy between the two proteins in the regulation of postnatal bone mass (17). Interestingly, in the double knock-out mice, the growth plate cartilage of the long bones was uncoupled with bone phenotype, with significantly delayed maturation of chondrocytes resulting in chondrodysplasia (17), suggesting a role for Hivep proteins in the promotion of chondrocyte differentiation. However, the mechanism by which Hivep proteins affect chondrogenesis remains unknown. In addition, to date, no information has been reported on the possible role of Hivep1 in osteogenesis and/or chondrogenesis.

In this study, *in vitro* analysis showed that, among the three Hivep proteins, only Hivep3 was inhibitory and that the others promoted osteoblast differentiation. In contrast, all three Hivep genes seemed to support chondrocyte differentiation in BMP-2-induced ATDC5 cells, suggesting their redundancy in chondrogenesis. We found that asparagine-linked glycosylation 2 (*Alg2*) is commonly down-regulated in BMP-2-induced osteoblast differentiation in both MC3T3-E1 and ST-2 cells. *Alg2* inhibited Runx2 activity without altering its protein level, resulting in suppression of osteoblast differentiation. Interestingly, in chondrogenesis of ATDC5 cells, Hivep3 induced the expression of cAMP-responsive element binding-protein 3-like 2 (*Creb3l2*), an endoplasmic reticulum (ER) stress transducer crucial for chondrogenesis (18), suggesting a possible role for Hivep3 in physiological mild ER stress. *Alg2* was also decreased by *Hivep3* knockdown in ATDC5 chondrocytes, whereas silencing of *Alg2* suppressed the expression of *Creb3l2* and chondrogenesis. To our knowledge, this study is the first to show a linkage between an asparagine-linked glycosylation mannosyltransferase gene and osteochondrogenesis.

EXPERIMENTAL PROCEDURES

Cell Culture and Differentiation—The mouse calvarial bone-derived osteoblast cell line, MC3T3-E1 (clone 4), and the mouse chondrogenic fibroblast cell line, C3H10T1/2, were obtained from the ATCC. The mouse bone marrow stromal cell line ST-2 and the mouse chondrogenic cell line ATDC5 were obtained from the RIKEN BioResource Center. MC3T3-E1 cells were cultured in minimum essential medium α (Invitrogen) containing 10% fetal bovine serum (FBS). ST-2 cells were cultured in RPMI 1640 medium (Sigma) containing 10% FBS. ATDC5 cells were cultured in Dulbecco's modified Eagle's medium (DMEM)/Ham's F-12 (1:1) (Invitrogen) containing 5% FBS. C3H10T1/2 cells were cultured in basal medium Eagle's (Sigma) with 2 mM L-glutamine and 10% FBS. COS-7 cells were purchased from RIKEN BioResource Center and maintained in DMEM supplemented with 10% FBS. All cell culture medium contained 100 units/ml penicillin G and 100 μ g/ml streptomycin. Cell differentiation was induced by the addition of recombinant human BMP-2 (PeproTech) at a concentration of 300 ng/ml. Micromass culture of ATDC5 cells was performed as described previously (19) to accelerate the maturation of chondrocyte differentiation.

Alkaline Phosphatase (ALP) and Alcian Blue Staining—The activity of ALP secreted into the extracellular matrix (ECM) of cultured cells was visualized with an ALP staining kit (85L-3R, Sigma). Cartilaginous glycosaminoglycans produced in the ECM by cultured cells were stained with Alcian blue 8GX (Sigma).

RNA Interference—Dharmacon siRNA ON-TARGETplus SMARTpool, a mixture of four independent siRNAs against mouse *Hivep1*, *Hivep2*, *Hivep3*, and *Alg2*, and the control reagent were purchased from Thermo Scientific. siRNAs were transfected into cells using Lipofectamine RNAiMax (Invitrogen).

Real Time Quantitative PCR—Cells were lysed with TRIzol reagent (Invitrogen) to purify RNA, and 1 μ g of total RNA was subjected to reverse transcription with the Verso cDNA kit (Thermo Scientific). The relative amounts of the gene transcripts were determined by real time quantitative PCR using SYBR premix Ex TaqII (Takara) and the Thermal Cycler Dice TP850 system (Takara). PCRs were performed in duplicate per sample, and the measured expression level of each gene was normalized to that of *Hprt1*. The sequence information for the primers used is listed in supplemental Table 1. All primer sets are for mouse genes, except for the m/h*Hivep3* primer set, which can be used to amplify both the mouse and human *Hivep3* genes. For evaluation of the tissue distribution of the Hivep genes and *Alg2* *in vivo*, tissues were harvested from 3-month-old mice, and mRNA was purified with TRIzol reagent before subjecting samples to qRT-PCR.

Microarray Analysis—Cells transfected with siRNA overnight were further incubated with BMP-2 for 2 days before being lysed with TRIzol reagent for mRNA purification. mRNA samples were cleaned up using the RNeasy MinElute Cleanup kit (Qiagen) and analyzed on a Mouse Gene 2.0 ST Array (Affymetrix) by BioMatrix Research.

Plasmids, Adenovirus, and Lentivirus—The mouse Hivep3 expression plasmid, pEF-Shn3, was a kind gift from Dr. Laurie Glimcher (Harvard Medical School). The human HIVEP3 expression plasmid pFN21A-HIVEP3 was obtained from Kazusa DNA Research Institute. The mouse type II Runx2 expression plasmid was a kind gift from Dr. Toshihisa Komori (Nagasaki University). The FLAG-Runx2-def expression plasmid has been described in our previous study (20). Mouse *Alg2* or *Runx2* cDNA was cloned from ST-2 cells by using a RT-PCR-based technique, subcloned into the entry vector, pENTR, and further transferred into the C-terminally V5-tagged expression vector, pEF-DEST51 (Invitrogen). For overexpression assays, cells were transfected with expression vectors using FuGENE 6 (Roche Applied Science) or Lipofectamine 2000 (Invitrogen). Cells transiently expressing the transgenes were selected and enriched by incubation with G418 disulfate (Nacalai Tesque) at a concentration of 250 $\mu\text{g}/\text{ml}$ for 3–7 days. To generate adenovirus-carrying *Alg2* cDNA, the *Alg2* gene in the pENTR-*Alg2* vector was transferred into the C-terminally V5-tagged adenovirus expression vector pAd/CMV/V5-DEST by LR recombination (Invitrogen) and was further transfected into the adenovirus-producing cell line 293A according to the manufacturer's protocol. The pAd/CMV/V5-GW/lacZ adenovirus expression vector was used to generate a control adenovirus. For generation of lentivirus carrying the *Alg2* gene, pENTR-*Alg2* and pENTR-5'EF1 α P were subjected to LR recombination with pLenti6.4/R4R2/V5-DEST (Invitrogen) to generate a lentiviral vector expressing C-terminally V5-tagged *Alg2* from the EF1 α promoter. The lentiviral expression vector or pLenti6/V5/GW-lacZ control vector was transfected into 293FT cells to generate the lentivirus. Virus infection into ST-2 cells was performed at a multiplicity of infection of 100. Cells infected with the lentivirus were selected by treatment with blasticidin S HCl (Invitrogen) at a concentration of 2.5 $\mu\text{g}/\text{ml}$. These experiments were approved by the Kagoshima University safety control committee for gene recombination techniques (number 22053).

Embryonic Bone Organ Culture—Calvarial bone and metatarsal bone (cartilage) rudiments were harvested from C57BL/6J mouse embryos at 17.5 days post-coitum (E17.5) and cultured in minimum essential medium α or DMEM/Ham's F-12 (1:1), respectively, supplemented with 10% FBS, 100 units/ml penicillin G, and 100 $\mu\text{g}/\text{ml}$ streptomycin, as described (21). The bone rudiments were incubated in virus solution overnight for infection of adenovirus or lentivirus. Cultured bones and cartilages were fixed in 96% ethanol and stained with 0.015% Alcian blue 8GX in a mixture solution of 96% ethanol/acetic acid (4:1) for 1 day, followed by a dehydration step in 100% ethanol. Dehydrated bones were immersed briefly in 1% potassium hydroxide (KOH), followed by staining in 0.001% alizarin red S (Sigma) in 1% KOH for 1 day. Images were captured with stereomicroscope M165FC (Leica). The animal experiments were approved by the Institutional Animal Care and Use Committee of Kagoshima University (number MD12137).

Immunoprecipitation and Immunoblotting—For immunoprecipitation assays, COS-7 cells were transfected with *Alg2*-V5 and/or FLAG-Runx2 plasmids and were lysed in M-PER lysis buffer (Thermo Scientific) supplemented with

aprotinin and phenylmethylsulfonyl fluoride (PMSF). The lysate was immunoprecipitated with anti-FLAG M2-agarose affinity gel (A2220, Sigma), and the M2 antibody-bound protein complex was eluted by incubation with 3 \times FLAG peptide (F4799, Sigma), according to the manufacturer's protocol. For immunoblotting assays, cells were lysed in either M-PER or NE-PER lysis buffer (Thermo Scientific) supplemented with aprotinin and PMSF or directly with 1 \times SDS sample buffer. SDS-PAGE, membrane transfer, and chemiluminescence were performed using a standard protocol. The blots were incubated with primary antibodies against *Alg2* (1:1000; LS-C81338, Lifespan Biosciences), *Runx2* (1:200; M-70, sc-10758, Santa Cruz Biotechnology), *Runx2* (1:1000; 8G5, MBL), *Sp7* (1:1000, ab22552, Abcam), *Ibsp* (1:1000, LS-C190916, Lifespan Biosciences), type II collagen (1:1000, LS-C175971, Lifespan Biosciences), *Creb3l2* (1:1000, ab76856, Abcam), *V5* (1:5000; R960-25, Invitrogen), FLAG (1:1000; M2, F1804, Sigma), and tubulin (1:1000; DM1A, T9026, Sigma) and with horseradish peroxidase (HRP)-conjugated anti-rabbit and anti-mouse secondary antibodies (1:10,000) (Cell Signaling). For examination of half-life of Runx2 protein, after overnight transfection with siRNA of *Hivep3*, ST-2 cells were treated with cycloheximide (Sigma) at 100 $\mu\text{g}/\text{ml}$, followed by immunoblotting using anti-Runx2 antibody. Signals were detected using the LAS 4000 mini image analyzer (Fujifilm).

Immunofluorescence—For immunofluorescence assays, cells transfected with Runx2 and/or *Alg2*-V5 expression plasmids were fixed with 4% paraformaldehyde in PBS for 30 min and treated with 0.2% Triton X-100. CAS block (Zymed Laboratories Inc.) was used for blocking. Cells were incubated with anti-Runx2 (1:100; 8G5, MBL), Alexa Fluor 568 rabbit anti-mouse IgG (1:1000; A11061, Invitrogen), and anti-V5-FITC (1:500; R619-25, Invitrogen) antibodies. Nuclei were stained with Hoechst dye (Invitrogen). Confocal fluorescent imaging was performed and analyzed using a laser scanning microscope system (LSM 700, Zeiss). For confirmation of the efficiency of virus infection in cultured bones, formalin-fixed mouse E17.5 embryo calvariae or metatarsal bones were embedded in paraffin blocks, which were sliced at a 4- μm thickness. The antigen was retrieved by Liberate Antibody Binding (L.A.B.) solution (Polysciences). A CAS block was used for blocking. Bone sections were incubated with anti-V5-FITC antibody. Images were captured with microscope AX80 and digital camera DP70 (Olympus).

Luciferase Assay—COS-7 cells or ST-2 cells were seeded in triplicate in 24-well plates and transiently transfected with the 6 \times OSE2 luciferase reporter plasmid (a kind gift from Dr. Toshihisa Komori), the mutant 6 \times OSE2 luciferase reporter plasmid (a kind gift from Dr. Gerard Karsenty, Columbia University Medical Center), the pGL4.75hRlucCMV *Renilla* vector (Promega), and expression vectors for Runx2, *Alg2*, or *Hivep3*. Dual-Luciferase assays were performed as described earlier (20) by using the GloMax 96 microplate luminometer (Promega).

Statistical Analysis—The data in this study have been expressed as mean \pm S.D. values of three independent experiments. Statistical comparisons between the different treatments were performed using an unpaired Student's *t* test in

Hivep3-dependent *Alg2* Expression Inhibits Osteogenesis

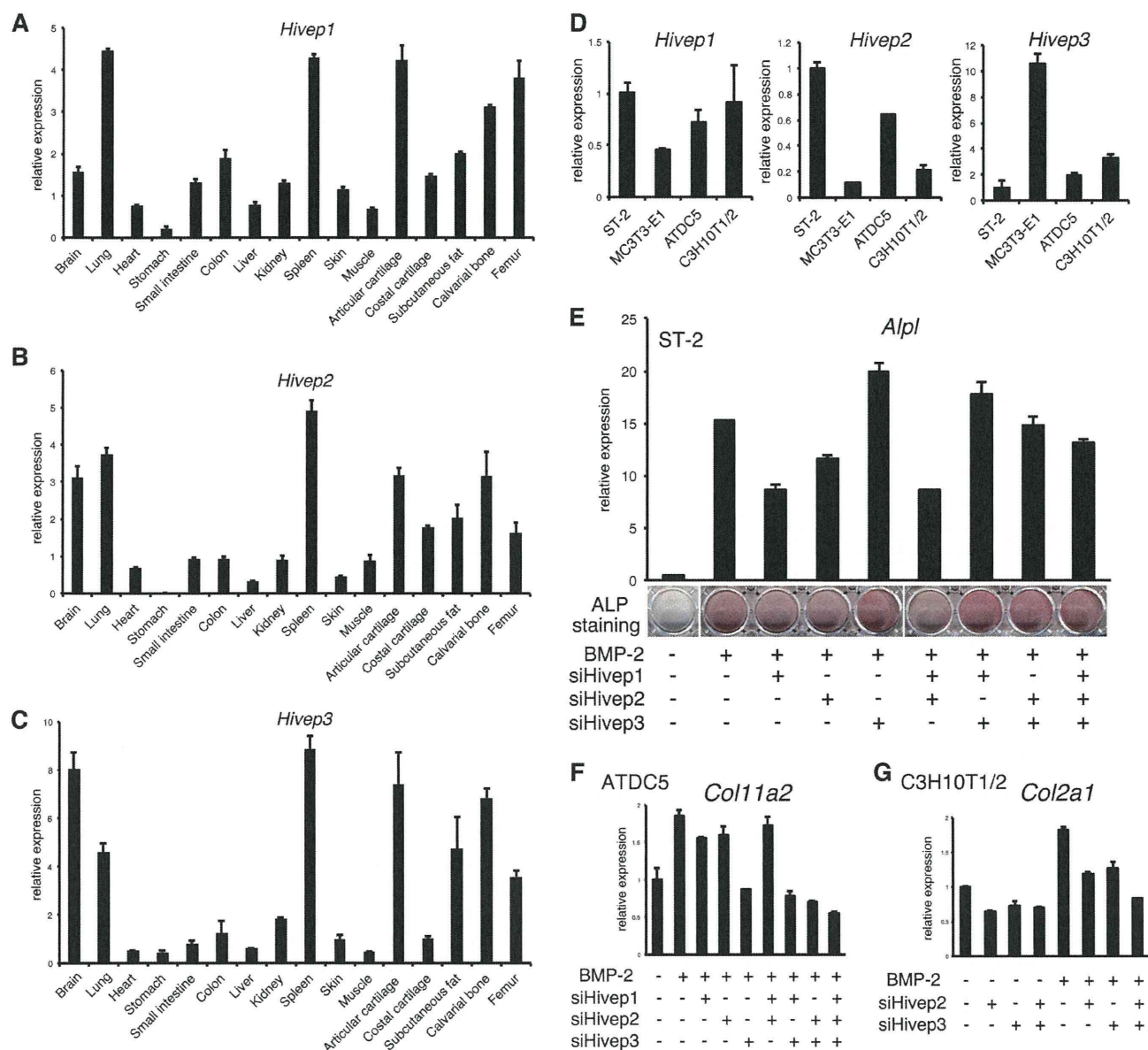


FIGURE 1. All three *Hivep* genes are expressed in bone and cartilage to support osteochondrogenesis except *Hivep3*, which is inhibitory for osteoblast differentiation. A–C, tissue cDNA panel of a 3-month-old mouse was subjected to quantitative RT-PCR (qRT-PCR) for *Hivep1* (A), *Hivep2* (B), or *Hivep3* (C). D, expression level of *Hivep1*, *Hivep2*, or *Hivep3* in the indicated cell lines was examined by qRT-PCR. E, ST-2 cells were transfected with siRNA for *Hivep1*, *Hivep2*, or *Hivep3* and treated with BMP-2 (300 ng/ml) for 6 days. Expression of *Alpl* was analyzed by qRT-PCR, and activity of ALP on ECM was visualized by ALP staining. F, ATDC5 cells were transfected with siRNA for *Hivep1*, *Hivep2*, and/or *Hivep3* and treated with BMP-2 (300 ng/ml) for 3 days. Expression of *Col11a2* was evaluated by qRT-PCR. G, C3H10T1/2 cells were transfected with siRNA for *Hivep2* and/or *Hivep3* and treated with BMP-2 (300 ng/ml) for 4 days. Expression of *Col2a1* was analyzed by qRT-PCR.

which $p < 0.05$ was considered significant, and $p < 0.01$ was considered highly significant.

RESULTS

Loss of *Hivep1* or *Hivep2* Suppresses Osteoblast Differentiation in ST-2 Cells, in Contrast to *Hivep3* Silencing, and All Three *Hivep* siRNAs Inhibited Chondrogenesis—The precise roles of *Hivep1* and *Hivep2* in osteoblast differentiation are unclear. In a tissue cDNA panel from a 3-month-old adult mouse, all the *Hivep* genes showed a relatively specific expression pattern with high expression being observed in the lung, spleen, artic-

ular cartilage, and bone (Fig. 1, A–C). However, the *in vitro* results for the osteochondrogenic cell lines ST-2, MC3T3-E1, ATDC5, and C3H10T1/2 showed that the expression profiles were completely different between the *Hivep* genes, with *Hivep1* being expressed ubiquitously, *Hivep2* abundant in ST-2 and ATDC5, and *Hivep3* prominent in MC3T3-E1 osteoblasts (Fig. 1D). If the *Hivep* genes cooperate in osteoblast differentiation, they should regulate some common sets of genes. To test this hypothesis, ST-2 cells transfected with siRNA for *Hivep1*, *Hivep2*, or *Hivep3* were analyzed by a microarray assay (supplemental Tables 2–4, respectively), and the results were com-

TABLE 1

Genes down-regulated by loss of the Hivep family genes

ST-2 cells were transfected with siRNA for *Hivep1*, *Hivep2*, or *Hivep3* and treated with BMP-2 (300 ng/ml) for 2 days. mRNA samples were subjected to microarray analysis. A, expression of five genes was commonly decreased by all the siRNAs for the three Hivep genes. B, expression of six genes was commonly down-regulated by the *Hivep1* and *Hivep2* siRNAs. C, expression of four genes was commonly down-regulated by the *Hivep1* and *Hivep3* siRNAs. D, expression of three genes was commonly down-regulated by the *Hivep2* and *Hivep3* siRNAs.

Unique Sorted Transcript ClusterID	siCont	siHivep1	siHivep2	siHivep3	gene symbol	gene description
17305520	21.529846	11.831301	9.75173	7.9562707	<i>Ear1</i>	eosinophil-associated, ribonuclease A family, member 1
17467150	24.856544	14.449716	11.51435	15.580148	<i>Vmn1r18</i>	vomer nasal 1 receptor 18
17444697	31.70125	19.534565	21.051311	17.505947	<i>Cyp3a59</i>	cytochrome P450, subfamily 3A, polypeptide 59
17245120	44.998398	29.873207	26.863188	29.873207	<i>1700030O20Rik</i>	RIKEN cDNA 1700030O20 gene
17481207	17.905426	10.739602	10.739602	10.603919	<i>Olfir608</i>	olfactory receptor 608

Unique Sorted Transcript ClusterID	siCont	siHivep1	siHivep2	gene symbol	gene description
17278822	65.41499	39.391872	41.367386	<i>Mir679</i>	microRNA 679
17302598	42.895184	26.84824	22.885633	<i>Gm6280</i>	predicted gene 6280
17344852	19.322012	12.227982	11.5472975	<i>Olfir97</i>	olfactory receptor 97
17509018	24.977375	16.012548	11.412771	<i>Adam34</i>	a disintegrin and metalloproteinase domain 34
17495404	82.13324	52.76455	42.29805	<i>Rps13</i>	ribosomal protein S13
17541719	21.694231	14.250495	14.178923	<i>Mir450-2</i>	microRNA 450-2

Unique Sorted Transcript ClusterID	siCont	siHivep1	siHivep3	gene symbol	gene description
17356739	63.32018	36.357323	32.77719	<i>Mir194-2</i>	microRNA 194-2
17268088	22.22885	13.294091	13.626566	<i>Gm11543</i>	predicted gene 11543
17324996	19.940779	12.472511	12.472511	<i>Mir1947</i>	microRNA 1947
17516159	30.844234	20.207043	19.56977	<i>Olfir251/Olfir900</i>	olfactory receptor 251 olfactory receptor 900

Unique Sorted Transcript ClusterID	siCont	siHivep2	siHivep3	gene symbol	gene description
17395379	248.2335	129.81422	142.53452	<i>LOC100504873</i>	zinc finger protein 14-like
17320035	82.69005	51.436905	49.273067	<i>Mir1249</i>	microRNA 1249
17366886	162.14816	104.84351	90.903786	<i>Mir467e</i>	microRNA 467e

pared. The expression of five genes decreased in all three knockdown experiments (Table 1, A), whereas six genes, four genes, or three genes were down-regulated in common by siHivep1 and siHivep2 (Table 1, B), siHivep1 and siHivep3 (Table 1, C), or siHivep2 and siHivep3 (Table 1, D), respectively, although no trend was observed in the purified genes. Moreover, none of the purified genes was reported to correlate with differentiation of osteoblasts or chondrocytes. To investigate the roles and possible synergism of the Hivep genes in osteoblast differentiation, the expression of the three Hivep genes was knocked down in ST-2 cells, alone or in combination (Fig. 1E). Although combined genetic ablation of the *Hivep2* and *Hivep3* genes in mice resulted in synergistically increased bone formation and bone volume (17), siRNA-mediated silencing of *Hivep2* in BMP-2-stimulated ST-2 cells decreased the expression and activity of ALP (Fig. 1E, compare lanes 2 and 4), whereas loss of *Hivep3* alone enhanced the osteoblast differentiation (Fig. 1E, compare lanes 2 and 5). Interestingly, combined transfection of siHivep2 with siHivep3 negated the enhancement of ALP production by *Hivep3* knockdown (Fig. 1E, compare lanes 2, 5, and 8). Similar to siHivep2, *Hivep1* siRNA inhibited ALP activity; however, there was no synergistic or additive effect on combined knockdown of *Hivep1* and *Hivep2*. These results suggest that, in ST-2 bone marrow stromal cells, the cell autonomous actions of Hivep genes are diverse and show no cooperation in osteoblast differentiation and that *Hivep1* and *Hivep2* promote the counteraction of the suppressive effect of

Hivep3. In contrast, in an siRNA-mediated knockdown assay in ATDC5 chondrocytes, siHivep1, siHivep2, and siHivep3 all decreased the BMP-2-induced expression of the chondrocyte-specific type XI collagen gene (*Col11a2*) (Fig. 1F). A similar result was observed in another chondrocytic cell line, C3H10T1/2, where knockdown of both *Hivep2* and *Hivep3* decreased the level of a chondrocyte marker, type II collagen gene (*Col2a1*) (Fig. 1G). In both experiments in chondrogenic cells, the combined loss of the Hivep genes showed some additive effects.

Hivep3 Suppresses Osteoblast Differentiation in Vitro—Although the mRNA level of *Runx2* was comparable between wild-type and *Hivep3* knock-out cells, the protein levels of *Runx2*, as well as the mRNA levels of the early osteoblast differentiation markers osterix (*Sp7*), alkaline phosphatase (*Alpl*), activating transcription factor 4 (*Atf4*), and bone sialoprotein (*Ibsp*) and of the late maturation marker osteocalcin (*Bglap2*) increased in knock-out osteoblasts (10). We first checked if this effect could be reproduced via siRNA-mediated knockdown in osteoblastic cell lines. We used the mouse bone marrow stromal cell line ST-2 as a model for premature osteoblast progenitors and MC3T3-E1 mouse calvaria-derived osteoblasts as mature osteoblasts. In both MC3T3-E1 and ST-2 cells, ~50% knockdown was achieved by transfection of siHivep3 (Fig. 2, A and C). As expected, *Hivep3* silencing did not have any effect on the mRNA expression of *Runx2* (Fig. 2, A and C). In ST-2 cells treated with cycloheximide to block *de novo* synthesis of *Runx2*

Hivep3-dependent *Alg2* Expression Inhibits Osteogenesis

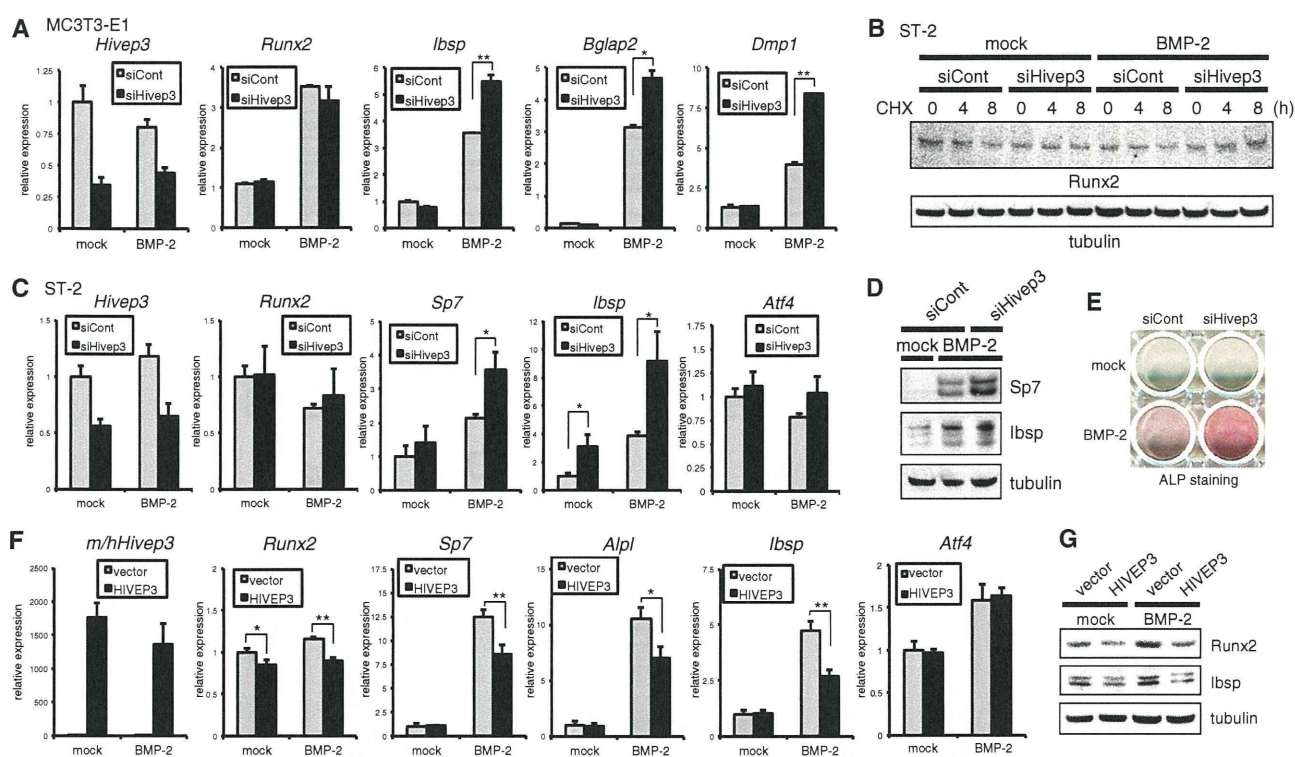


FIGURE 2. Silencing of *Hivep3* increases protein stability of Runx2 to promote BMP-2-induced osteoblast differentiation. *A*, MC3T3-E1 osteoblasts were transfected with siRNA for *Hivep3* with or without BMP-2 treatment (300 ng/ml) for 6 days. qRT-PCR analysis was performed for the indicated genes. *B*, siRNA-transfected ST-2 cells were treated with 100 μ g/ml cycloheximide (CHX) with or without BMP-2 treatment (300 ng/ml) for the indicated time points. Cell lysates were analyzed by immunoblotting with an anti-Runx2 antibody. Tubulin served as a loading control. *C*, ST-2 cells were transfected with siRNA for *Hivep3* with or without BMP-2 treatment (300 ng/ml) for 3 days. The expression level of the indicated genes was examined by qRT-PCR. *D*, ST-2 cells were transfected with siRNA for *Hivep3* with BMP-2 treatment (300 ng/ml) for 7 days. Cell lysates were analyzed by immunoblotting with the indicated antibodies. Tubulin served as a loading control. *E*, ST-2 cells were transfected with *Hivep3* siRNA and stimulated with BMP-2 (300 ng/ml) for 6 days. ALP staining was performed. *F*, ST-2 cells were transfected with a human HIVEP3 expression vector and further stimulated with BMP-2 (300 ng/ml) for 4 days. The expression of the indicated genes was evaluated by qRT-PCR. *G*, ST-2 cells transfected with a human HIVEP3 expression vector were stimulated with BMP-2 (300 ng/ml) for 5 days. Cell lysates were analyzed by immunoblotting with the indicated antibodies. Tubulin served as the indicated control. $^*p < 0.05$; $^{**}p < 0.01$.

protein, the protein level of Runx2 decreased in a time-dependent manner (Fig. 2*B*), although the protein expression was maintained in siHivep3-transfected cells. Moreover, combined induction of BMP-2 and siHivep3 in ST-2 cells increased Runx2 protein in a time-dependent fashion (Fig. 2*B*). Therefore, siRNA-mediated silencing of *Hivep3* stabilized Runx2 protein. As a result, expression of *Sp7*, *Ibsp*, and *Bglap2* was up-regulated in MC3T3-E1 and ST-2 cells (Fig. 2, *A* and *C*). In addition, the expression of an osteocyte marker, dentin matrix protein 1 (*Dmp1*), was elevated by *Hivep3* knockdown in MC3T3-E1 osteoblasts (Fig. 2*A*). The siHivep3-mediated increase of osteoblastic differentiation in ST-2 cells was confirmed by immunoblotting against *Sp7* and *Ibsp* (Fig. 2*D*) or ALP staining (Fig. 2*E*). We introduced the human *HIVEP3* gene in ST-2 cells through transfection and confirmed the transgene expression by qRT-PCR (Fig. 2*F*). HIVEP3 suppressed BMP-2-induced osteoblast differentiation (Fig. 2, *F* and *G*) and protein expression of Runx2 (Fig. 2*G*). Interestingly, the mRNA expression of *Runx2* decreased following transfection with HIVEP3. As HIVEP3 destabilizes Runx2 protein, this result is likely due to loss of auto-induction of Runx2 (22), in which endogenous Runx2 mRNA expression increased in Runx2 transgenic mice (23). In both cases of knockdown and overexpression of *Hivep3*,

expression of *Atf4* did not change (Fig. 2, *C* and *F*), although it increased in *Hivep3* knock-out osteoblasts (10).

Reduced *Alg2* Gene Expression Following Knockdown of *Hivep3*—We next screened for genes whose expression was commonly reduced in both ST-2 cells and MC3T3-E1 cells upon *Hivep3* silencing by microarray analysis. The genes with decreased expression in MC3T3-E1 or ST-2 cells by >1.5-fold are listed in supplemental Table 5 (38 genes) or supplemental Table 4 (74 genes), respectively. Among these genes, only five were commonly down-regulated by siHivep3 in the two cell lines (Fig. 3*A*). For more stringent screening, we further increased the cutoff threshold to a >1.8-fold decrease, which left two genes each in the two cell lines, *Lypla2* and *Alg2* in MC3T3-E1 cells and *Alg2* and *Igfbp5* in ST-2 cells (Fig. 3*A*). Therefore, *Alg2* most commonly showed a decrease in expression due to *Hivep3* knockdown in both MC3T3-E1 and ST-2 cells. Asparagine-linked glycosylation (ALG) is one of the most common protein modification reactions in eukaryotic cells, as many proteins that are translocated across or integrated into the rough ER carry *N*-linked oligosaccharides (24). *Alg2* is an α -1,3-mannosyltransferase forming a type I transmembrane protein on the ER, with its active site being cytosolically oriented (25). To date, no information has been reported to link

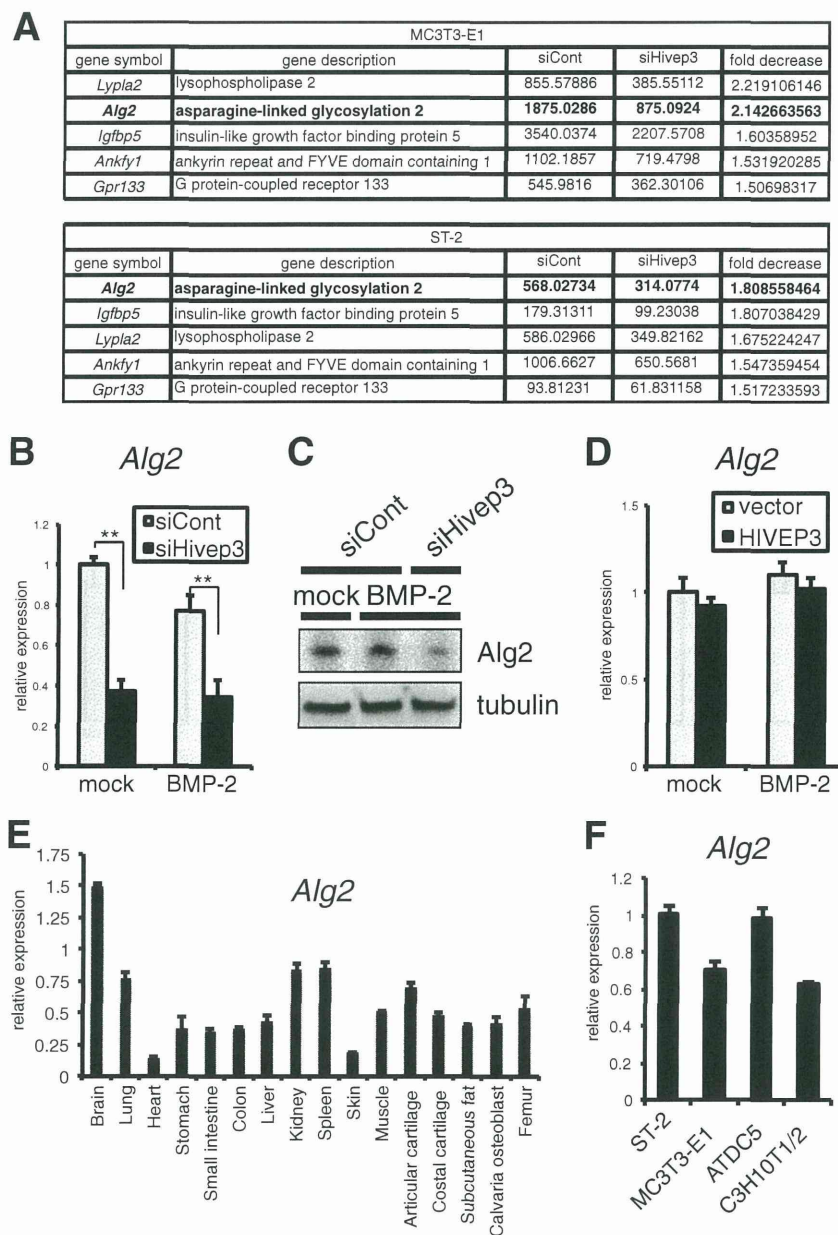


FIGURE 3. Expression of the *Alg2* gene is reduced upon knockdown of *Hivep3* in osteoblastic cells. *A*, siRNA for *Hivep3* was transfected into MC3T3-E1 or ST-2 cells prior to treatment with BMP-2 (300 ng/ml) for 2 days and analyzed by microarray. A list of five genes with decreased signal intensity, in common between MC3T3-E1 and ST-2 cells, is presented. *B*, ST-2 cells were transfected with siRNA for *Hivep3* with or without BMP-2 treatment (300 ng/ml) for 3 days. The expression level of *Alg2* was examined by qRT-PCR. *C*, ST-2 cells were transfected with siRNA for *Hivep3* with BMP-2 treatment (300 ng/ml) for 7 days. Cell lysates were analyzed by immunoblotting with an anti-*Alg2* antibody. Tubulin served as a loading control. *D*, ST-2 cells were transfected with a human HIVEP3 expression vector to be stimulated with BMP-2 (300 ng/ml) for 4 days. The expression of *Alg2* was evaluated by qRT-PCR. *E*, tissue cDNA panel of a 3-month-old mouse was subjected to real time PCR for *Alg2*. *F*, expression level of *Alg2* in the indicated cell lines was examined by a qRT-PCR assay. **, $p < 0.01$.

Alg2 to cell differentiation. We confirmed the microarray results by qRT-PCR (Fig. 3*B*) or immunoblotting (Fig. 3*C*) and verified that knockdown of *Hivep3* in ST-2 cells decreased the level of *Alg2* by over 50%. However, forced expression of HIVEP3 did not increase *Alg2* expression (Fig. 3*D*). We next examined the tissue distribution of *Alg2* in 3-month-old mice by quantitative PCR analysis of a tissue cDNA panel (Fig. 3*E*). In tissues with low expression of *Hivep3* (Fig. 1*C*), *i.e.* the heart or skin, *Alg2* also showed a minimum level of expression, although

both genes were highly expressed in the brain and lungs, suggesting a linkage between the levels of the two genes. However, there were some exceptions, *e.g.* *Hivep3* was expressed at high levels in fat, cartilage, and bone, whereas *Alg2* was detected at a moderate level in these tissues. From the osteoblastic and/or chondrocytic cell lines, MC3T3-E1 showed a significantly high level of *Hivep3* expression (Fig. 1*D*), whereas *Alg2* was detected in a relatively ubiquitous pattern (Fig. 3*F*). These results suggest that *Hivep3* is essential but not sufficient for the expression of *Alg2*.